Thermal atomic layer etching of HfO_2 using HF for fluorination and $TiCl_4$ for ligand-exchange

Younghee Lee[1] and Steven M. George[1,2]
[1]*Department of Chemistry and Biochemistry, University of Colorado, Boulder, Colorado 80309-0215*
[2]*Department of Mechanical Engineering, University of Colorado, Boulder, Colorado 80309-0215*

(Received 17 June 2018; accepted 28 August 2018; published 25 September 2018)

Thermal atomic layer etching (ALE) can be accomplished using sequential fluorination and ligand-exchange reactions. HF has been a typical fluorination reactant. Various metal reactants have been used for ligand-exchange, such as $Sn(acac)_2$, $Al(CH_3)_3$, $AlCl(CH_3)_2$, and $SiCl_4$. This study explored $TiCl_4$ as a new metal chloride reactant for ligand-exchange. Thermal HfO_2 ALE using HF and $TiCl_4$ as the reactants was studied using *in situ* quartz crystal microbalance (QCM) measurements from 200 to 300 °C. The HfO_2 films were etched linearly versus the number of HF and $TiCl_4$ reaction cycles. The sequential HF and $TiCl_4$ reactions were also self-limiting versus reactant exposure. The QCM studies observed a mass change per cycle (MCPC) of −10.2 ng/(cm^2 cycle) at 200 °C and −56.4 ng/(cm^2 cycle) at 300 °C. These MCPCs correspond to HfO_2 etch rates of 0.11 Å/cycle at 200 °C and 0.59 Å/cycle at 300 °C. To explore the selectivity of thermal ALE using HF and $TiCl_4$ as the reactants, spectroscopic ellipsometry (SE) measurements were also employed to survey the etching of various materials. The SE results revealed that HfO_2 and ZrO_2 were etched by HF and $TiCl_4$. In contrast, Al_2O_3, SiO_2, Si_3N_4, and TiN were not etched by HF and $TiCl_4$. The etching selectivity can be explained by the reaction thermochemistry and the stability and volatility of the possible etch products. Al_2O_3 can also serve as an etch stop for HfO_2 ALE. *Published by the AVS.*
https://doi.org/10.1116/1.5045130

I. INTRODUCTION

Atomic layer etching (ALE) can remove material based on sequential, self-limiting surface reactions.[1,2] ALE is the reverse of atomic layer deposition (ALD).[3,4] ALE can remove thin films with atomic layer control. Together, ALD and ALE can provide the processing techniques that are required for film growth and removal at the atomic level. This atomic scale control over the growth and removal of dielectric, semiconductor and conducting materials is needed for the fabrication of nanoscale devices.[5]

ALE can be accomplished using both plasma and thermal methods. Plasma ALE techniques use ion-enhanced or energetic noble gas atom-enhanced surface reactions.[1,2] During plasma ALE, a halogen or fluorocarbon film is typically adsorbed on the surface of the material. After halogen or fluorocarbon film adsorption, ion or noble gas atom bombardment is used to desorb halogen or carbon compounds that etch the material.[1] Using this approach, plasma ALE has been reported for Si,[6–8] Ge,[9] and various compound semiconductors.[10,11] Plasma ALE has also been demonstrated for various oxides and nitrides, such as SiO_2,[12,13] Si_3N_4,[14,15] and HfO_2.[16,17] Other plasma ALE studies have been performed on different carbon substrates.[18,19]

Thermal ALE techniques have also been demonstrated using sequential, self-limiting gas phase reactions. One thermal ALE approach utilizes fluorination and ligand-exchange reactions.[4,20] HF has been used as the fluorination reactant that converts the metal compound to a metal fluoride. A variety of metal reactants have been employed for ligand-exchange, such as $Sn(acac)_2$, $Al(CH_3)_3$, $AlCl(CH_3)_2$, and $SiCl_4$.[21] The ligand-exchange reaction is able to volatilize the metal fluoride. Thermal ALE using fluorination and ligand-exchange has been reported for a wide range of materials, including Al_2O_3,[20,22–24] HfO_2,[25] ZrO_2,[21] AlF_3,[26] and AlN.[27]

Various conversion mechanisms for thermal ALE have also been developed that convert the surface layer of the initial material to a different material that can be removed by either fluorination to a volatile fluoride or fluorination and ligand-exchange. Thermal ALE using a conversion mechanism has been demonstrated for SiO_2,[22] ZnO,[28] and WO_3.[29] Additional mechanisms for the thermal ALE of TiN (Ref. 30) and W (Ref. 31) are based on oxidation and then fluorination to a volatile fluoride. Oxidation can also be employed together with conversion and fluorination to a volatile fluoride for W ALE.[29] Oxidation can also be utilized together with thermal volatilization by organic reactants for Fe, Co, Pd, and Pt ALE.[32] Other thermal ALE mechanisms have been developed for TiO_2 ALE that are based on the temperature-dependent volatility of metal oxyfluorides and oxychlorides.[33]

HfO_2 is a high k dielectric material that is employed as the gate oxide in metal oxide semiconductor field effect transistors (MOSFETs).[34] The HfO_2 films in the gate stack are typically grown using ALD. The HfO_2-based gate oxide was initially employed at the 45 nm node in complementary MOSFETs.[35] HfO_2 is also used as the gate dielectric in FinFETs (Ref. 36) and can be utilized as the gate dielectric in nanowire transistors.[37] HfO_2 etching may be needed to reduce the thickness of the gate dielectric.[16] In addition, HfO_2 etching can also smooth the gate dielectric surface. Plasma HfO_2 ALE has been developed using chlorine adsorption on the HfO_2 substrate and then energetic Ar beams to desorb Cl-containing compounds.[16] Thermal HfO_2

ALE has also been demonstrated using fluorination and ligand-exchange reactions using HF and either $Sn(acac)_2$, $Al(CH_3)_3$, $AlCl(CH_3)_2$, or $SiCl_4$ as the metal reactant.[21,25]

This paper presents a new approach to thermal HfO_2 ALE using sequential, self-limiting reactions with HF and $TiCl_4$ as the reactants. $TiCl_4$ as the metal reactant may display advantages compared with $Sn(acac)_2$ such as higher thermal stability. $TiCl_4$ may also display different selectivity in etching relative to $Sn(acac)_2$, $Al(CH_3)_3$, $AlCl(CH_3)_2$, or $SiCl_4$ as the metal reactant. Many of the studies employ *in situ* quartz crystal microbalance (QCM) measurements to obtain the HfO_2 etch rates and the mass changes after the HF and $TiCl_4$ exposures. The mass change per cycle (MCPC) and the individual mass changes after the HF and $TiCl_4$ exposures help to define a mechanism for HfO_2 ALE. In addition, the selectivity of the HF and $TiCl_4$ reactants for etching HfO_2, ZrO_2, Al_2O_3, SiO_2, Si_3N_4, and TiN is established using spectroscopic ellipsometry (SE) studies. Al_2O_3 is also demonstrated as an etch stop for thermal HfO_2 ALE.

II. EXPERIMENT

A. Substrate preparation

The growth of HfO_2 films for the *in situ* QCM experiments was conducted using HfO_2 ALD at 200–300 °C with tetrakis(dimethylamido) hafnium (TDMAH; 99.99%, Sigma-Aldrich) and deionized H_2O. The TDMAH was transferred to a stainless steel bubbler in a dry N_2-filled glove bag. The stainless steel bubbler temperature for TDMAH was held at 67 °C. The TDMAH pressure transients were 5–10 mTorr. The glass bubbler containing water was degassed by freeze-pump-thaw cycles and was maintained at room temperature. The growth of the Al_2O_3 ALD thin films for the *in situ* QCM experiments was conducted using trimethylaluminum (TMA; 97%, Sigma-Aldrich) and H_2O at 250 °C.

The Al_2O_3, HfO_2, ZrO_2, SiO_2, Si_3N_4, and TiN thin films on silicon wafers for the *ex situ* spectroscopic ellipsometry studies were provided by SEMATECH.[21] The Al_2O_3, HfO_2, ZrO_2, and TiN films were prepared by semiconductor ALD processes in commercial tools. The SiO_2 and Si_3N_4 films were deposited by chemical vapor deposition in a high volume single wafer tool. The thickness of all the initial films was targeted to be ~50 Å. Actual thicknesses were in the range of 39−68 Å as determined by SE measurements.

B. Etching reactants

HF-pyridine [HF-pyridine (70 wt%), Sigma-Aldrich] was used as the fluorination reactant. HF-pyridine enables the safe handling of anhydrous HF. HF-pyridine is a liquid at room temperature and is known as Olah's reagent.[38] The HF-pyridine solution has an equilibrium with gaseous HF. HF dominates the vapor pressure of HF-pyridine.[25] Previous mass spectrometer analysis has shown that the HF pressure over the HF-pyridine solution is 90–100 Torr at room temperature.[25] Mass signals for pyridine were not detected by the mass spectrometer during HF exposures.[39] The HF-pyridine was transferred to a gold-coated stainless steel bubbler in a dry N_2-filled glove bag. The HF-pyridine precursor was maintained at room temperature. A variable conductance valve was adjusted to produce HF pressure transients of 80 mTorr during the HF exposures.

Titanium tetrachloride ($TiCl_4$, 99.0% Fluka) was transferred to a glass bubbler in a dry N_2-filled glove bag and maintained at room temperature. $TiCl_4$ has a vapor pressure of ~10 Torr at 20 °C. A variable conductance valve was adjusted to produce $TiCl_4$ pressure transients of 120 mTorr during the $TiCl_4$ exposures.

C. Viscous flow reactor equipped for *in situ* QCM measurements

A viscous flow reactor was used to perform the ALE reactions.[40] The details of this reactor for thermal ALE experiments have been described previously.[20,24,25,30] Briefly, a proportional-integral-derivative temperature controller (2604, Eurotherm) held the temperature within ±0.04 °C for accurate QCM measurements. The QCM RC crystal (gold coated and polished, 6 MHz, Colnatec) was positioned in a sensor head (BSH-150, Inficon). The sensor head was also sealed with high temperature epoxy (Epo-Tek H21D, epoxy technology) to prevent deposition on the back side of the QCM crystal.[40] The QCM measurements were recorded using a thin film deposition monitor (Maxtek TM-400, Inficon).

A mechanical pump (Pascal 2015SD, Alcatel) was used to pump the reactor. A constant total flow of 150 sccm of ultrahigh purity N_2 carrier gas into the reactor was delivered by three separate mass flow controllers (Type 1179A, MKS). Additional N_2 gas flow of 20 sccm was provided using a metering bellows-sealed valve (SS-4BMG, Swagelok) to prevent deposition on the backside of the QCM crystal.[40] A base pressure of ~1 Torr in the reactor was produced by the total N_2 gas flow of 170 sccm.

D. Spectroscopic ellipsometry measurements

The thicknesses of the various thin films on the Si wafers were determined by SE measurements. A spectroscopic ellipsometer (M-2000, J. A. Woollam) measured Ψ and Δ at 240−1700 nm with an incidence angle of 75°. The analysis software (CompleteEASE, J. A. Woollam) fitted Ψ and Δ at 240−900 nm to determine the thickness and refractive index of the film. A Sellmeier model was used for fitting the thickness of the Al_2O_3, HfO_2, ZrO_2, SiO_2, and Si_3N_4 films.[41] A Lorentz model was used for fitting the TiN film.

III. RESULTS AND DISCUSSION

A. HfO_2 ALE using HF and $TiCl_4$

HfO_2 ALE was studied by QCM measurements using sequential exposures of HF and $TiCl_4$ reactants. Figure 1 shows the mass change during 80 cycles of HfO_2 ALE at 250 °C. The initial HfO_2 film on the QCM crystal was grown by 100 cycles of HfO_2 ALD using TDMAH and H_2O at 250 °C. The HfO_2 film was then etched with 80 ALE cycles consisting of sequential HF and $TiCl_4$ exposures. Each ALE cycle was defined by an HF exposure of 1 s, a first N_2 purge

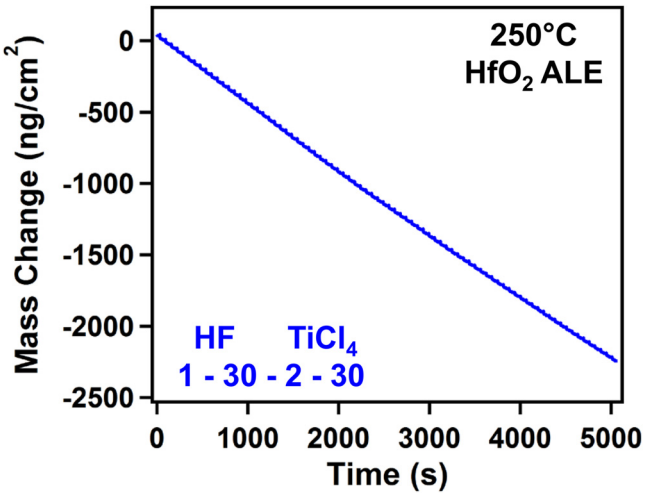

FIG. 1. Mass change vs time for HfO_2 ALE using 80 sequential HF and $TiCl_4$ exposures at 250 °C using the reaction sequence of (1−30−2−30).

of 30 s, a $TiCl_4$ exposure of 2.0 s, and a second N_2 purge of 30 s. This reaction sequence is expressed as 1−30−2−30. The HF and $TiCl_4$ exposures were both long enough for self-limited reactions in the saturation regime. The linear etching versus the number of HF and $TiCl_4$ exposures during HfO_2 ALE shown in Fig. 1 yields a MCPC of −27.4 ng/(cm^2 cycle). This MCPC corresponds to an etch per cycle of 0.29 Å/cycle based on the HfO_2 ALD film density of 9.6 g/cm^3 measured by X-ray reflectivity (XRR).[25]

Figure 2 shows an enlargement of the mass change during three sequential cycles of HF and $TiCl_4$ exposures for HfO_2 ALE at 250 °C. The mass loss with the HF exposure of 1 s is $\Delta M_{HF} = -5.9$ ng/(cm^2 cycle). The fluorination of HfO_2 to HfF_4 by HF should occur spontaneously and lead to a mass increase[42]

$$HfO_2(s) + 4HF(g) \rightarrow HfF_4(s) + 2H_2O(g), \quad \Delta G^\circ = -16.0 \text{ kcal/mol at } 250\,^\circ\text{C}. \tag{1}$$

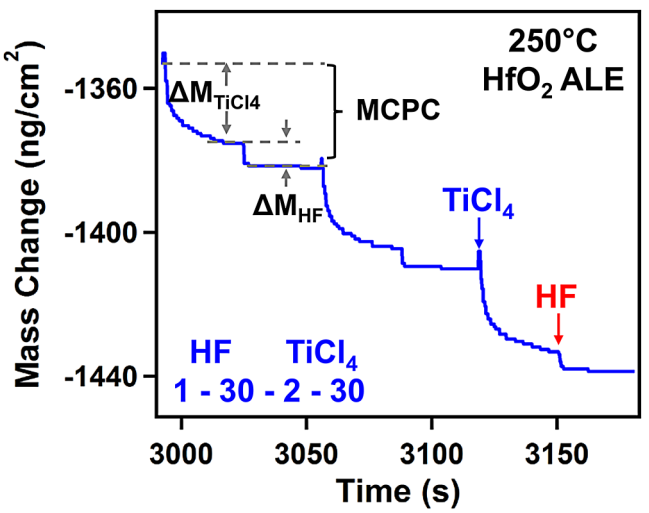

FIG. 2. Enlargement of the linear region of Fig. 1 showing the individual mass changes for three HfO_2 ALE cycles.

This fluorination reaction will result in a mass increase of 12% from 210.5 amu for HfO_2 to 254.5 amu for HfF_4. The overall mass loss of $\Delta M_{HF} = -5.9$ ng/(cm^2 cycle) indicates that the replacement of chlorine by fluorine is also occurring during the HF exposure. The chlorine surface species are present as a result of the previous $TiCl_4$ reaction.

The exchange of Cl with F from HF is a thermochemically favorable reaction. This Cl/F exchange can be modeled by the fluorination reaction[42]

$$HfCl_4(s) + 4HF(g) \rightarrow HfF_4(s) + 4HCl(g), \quad \Delta G^\circ = -48.2 \text{ kcal/mol at } 250\,^\circ\text{C}. \tag{2}$$

Cl/F exchange leads to an overall mass loss resulting from the higher atomic mass of Cl compared with F (35.5 vs 19.0 amu). The fluorination of $HfCl_4$ to HfF_4 will result in a mass decrease of 26% from 320.3 amu for $HfCl_4$ to 254.5 amu for HfF_4. The competition between a mass increase for HfO_2 fluorination and a mass decrease for Cl/F exchange leads to an overall mass loss of $\Delta M_{HF} = -5.9$ ng/(cm^2 cycle) after the HF exposure.

The mass loss with the 2 s of $TiCl_4$ exposure is $\Delta M_{TiCl_4} = -21.5$ ng/(cm^2 cycle). This mass loss is consistent with the removal of the HfF_4 surface layer by the $TiCl_4$ reaction. The HfF_4 layer was formed by the previous HF fluorination reaction. $TiCl_4$ transfers Cl to the HfF_4 surface layer and may produce volatile $HfF_{4-y}Cl_y$ and $TiCl_{4-z}F_z$ etch products.

The ligand-exchange reaction may not yield complete F/Cl exchange to produce $HfCl_4$ and TiF_4. Thermochemical calculations for the standard free energy change, ΔG°, do not predict a spontaneous reaction if the reaction products are $HfCl_4$ and TiF_4.[42]

$$HfF_4(s) + TiCl_4(g) \rightarrow HfCl_4(g) + TiF_4(g), \quad \Delta G^\circ = +34.1 \text{ kcal/mol at } 250\,^\circ\text{C}. \tag{3}$$

Mixed metal chlorides/fluorides, such as $HfF_{4-y}Cl_y$ and $TiCl_{4-z}F_z$, are the likely etch products if the mixed metal halides are volatile at the reaction temperature. These mixed metal chloride/fluoride species may have more favorable thermochemistry. Mass spectrometry analysis is required to confirm the identity of the volatile etch products.

Figure 3 displays the self-limiting behavior of the HF and $TiCl_4$ reactions during HfO_2 ALE. The HF and $TiCl_4$ exposures were defined by minidoses that were less than the exposures required for self-limited exposures in the saturation regime. The minidoses in Fig. 3 were reactant exposures for 0.5 s at pressures of ≤80 mTorr for HF and ≤120 mTorr for $TiCl_4$.

ΔM_{HF} reveals a small mass loss and levels off at 250 and 300 °C as shown in Fig. 3(a). This behavior is consistent with the favorable fluorination exchange of chlorine surface species and the fluorination of HfO_2 to HfF_4. The first minidose of HF is responsible for Cl/F exchange and produces the largest mass decrease. The minidoses after the first HF minidose can then contribute by producing additional Cl/F exchange and also fluorination of HfO_2.

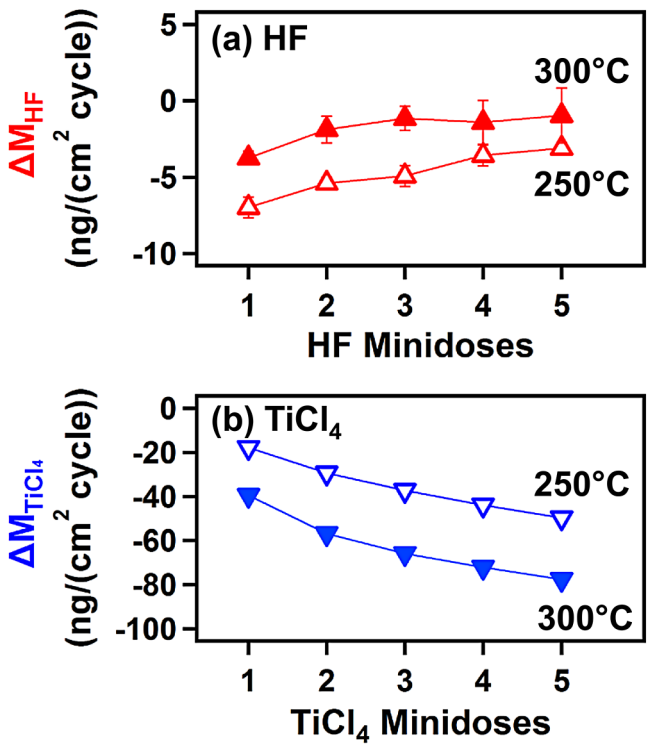

FIG. 3. (a) Mass change after HF exposure (ΔM_{HF}) vs HF exposure time at 250 and 300 °C. (b) Mass change after $TiCl_4$ exposure (ΔM_{TiCl_4}) vs $TiCl_4$ exposure time at 250 and 300 °C.

The fluorination of the underlying HfO_2 film by subsequent HF minidoses to form additional HfF_4 leads to a mass increase. Consequently, these multiple HF minidoses produce smaller negative ΔM_{HF} values. The fluorination of HfO_2 is self-limiting because the HfF_4 surface layer forms a diffusion barrier to subsequent fluorination by HF. The self-limiting nature of HfO_2 fluorination is similar to the self-limiting oxidation of silicon defined by Deal–Grove kinetics.[43]

Figure 3(b) displays the mass change after multiple minidoses of $TiCl_4$ at 250 °C. After multiple $TiCl_4$ minidoses, ΔM_{TiCl_4} displays a mass loss and becomes larger as more HfF_4 is removed by $TiCl_4$. The mass changes after many $TiCl_4$ minidoses level off but do not reach a distinct limiting value at 250 °C. The slow desorption of $HfF_{4-y}Cl_y$ etch products from the surface may be responsible for this behavior. This behavior after multiple $TiCl_4$ minidoses is similar when the reaction temperature is elevated to 300 °C. Longer purge times after $TiCl_4$ exposures may lead to better saturation behavior.

Figure 4 illustrates the proposed reaction mechanism for HfO_2 ALE using HF and $TiCl_4$ as the reactants. This proposed reaction mechanism is based on the mass changes during the HF and $TiCl_4$ exposures as revealed by the QCM experiments. This schematic does not show the surface species that do not change. For example, HfF_x species that are not removed by $TiCl_4$ and $HfCl_y$ species that are not exchanged by HF may be present for the entire reaction.

In the fluorination reaction (a), Fig. 4 shows that HF reacts with Cl surface species to form F surface species and HCl reaction products. HF also reacts with the underlying HfO_2 film to produce an HfF_4 surface layer and H_2O reaction products. There is also a possibility that OH species could remain on the surface if the H_2O desorption kinetics are not favorable.

In the ligand-exchange reaction (b), Fig. 4 shows that $TiCl_4$ interacts with the HfF_4 surface layer to form volatile $HfCl_4$ and TiF_4 reaction products. Mixed hafnium fluoride/

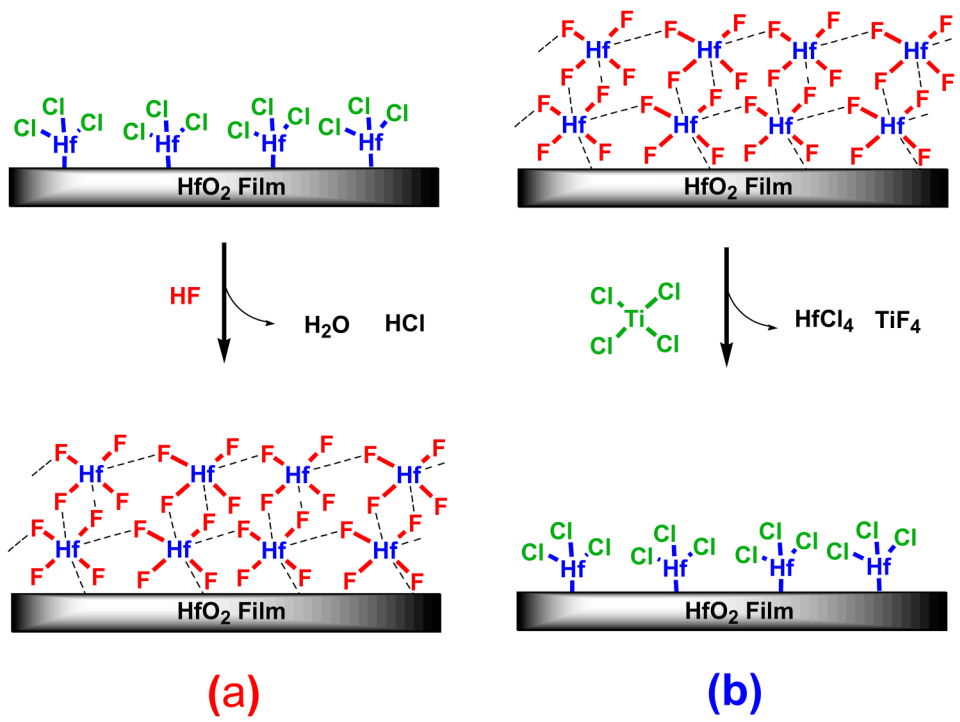

FIG. 4. Schematic of the proposed reaction mechanism for HfO_2 ALE showing (a) HF reaction and (b) $TiCl_4$ reaction.

chloride species, such as $HfFCl_3$, HfF_2Cl_2, and HfF_3Cl, are also likely as etch products if they have high enough vapor pressure at 250 °C. Mixed titanium fluoride/chloride species may also appear as etch products if they are volatile. $HfCl_4$ is volatile having a vapor pressure >1 Torr at 200 °C. The sublimation temperature of $HfCl_4$ is 317 °C. TiF_4 is also volatile having a vapor pressure >1 Torr at 160 °C.[44]

B. Temperature dependence of HfO_2 ALE

Figure 5 displays the mass change during HfO_2 ALE cycles at 200, 225, 250, 275, and 300 °C with the HF and $TiCl_4$ reaction sequence of 1–30–2–30. The initial HfO_2 ALD films were prepared by 100 cycles of HfO_2 ALD at the same temperatures as the ALE reactions. The linear etching of the HfO_2 films versus the number of ALE cycles was observed at all temperatures. The MCPC becomes larger with temperature from −10.2 ng/(cm^2 cycle) at 200 °C to −56.4 ng/(cm^2 cycle) at 300 °C. These MCPCs are consistent with etch rates that increase from 0.11 Å/cycle at 200 °C to 0.59 Å/cycle at 300 °C. These etch rates were determined using a HfO_2 film density of 9.6 g/cm^3.[25]

Figure 6 shows the ΔM_{HF}, ΔM_{TiCl_4}, and MCPC values at 200–300 °C. The ΔM_{HF} values show a mass loss at 200 °C, and the mass loss becomes slightly smaller at higher temperatures. The fluorination of more HfO_2 to HfF_4 probably is responsible for the smaller negative ΔM_{HF} values at high temperatures. The ΔM_{TiCl_4} values are consistent with $TiCl_4$ removing more of the HfF_4 layer at higher temperatures. The larger removal of HfF_4 by $TiCl_4$ leads to a higher HfO_2 etch rate at high temperature.

The Arrhenius plot of ln(−MCPC) vs 1000/T is shown in Fig. 7. This Arrhenius plot yields an activation barrier $E_a = 9.5 \pm 0.4$ kcal/mol. Because the temperature dependence of the MCPC is largely determined by ΔM_{TiCl_4}, this activation barrier is more closely tied to the ligand-exchange reaction. The ligand-exchange reaction is believed to occur via a four-center ring transition state. The activation barrier could be related to the transition state for this four-center ring reaction. Alternatively, the activation barrier could be defined more by the desorption barrier to remove the etch products from the surface.

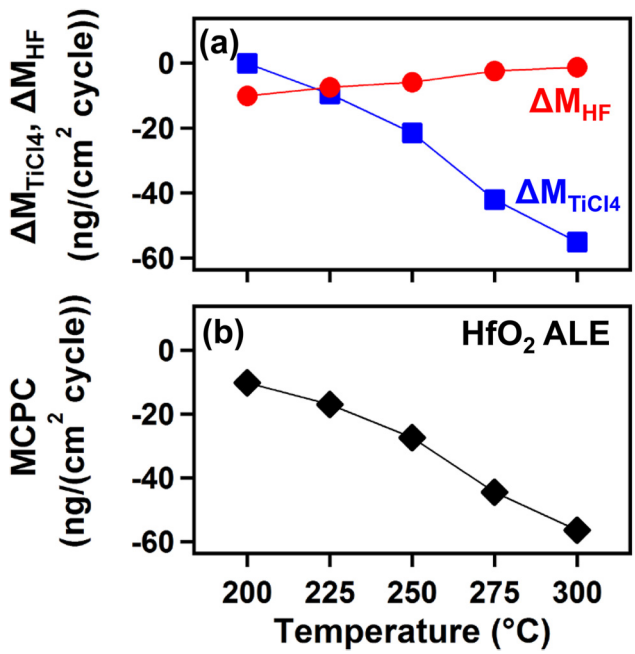

FIG. 6. Temperature dependence of (a) ΔM_{HF} and ΔM_{TiCl_4} and (b) MCPC for Al_2O_3 ALE.

The individual ΔM_{HF}, ΔM_{TiCl_4}, and MCPC values are listed in Table I. The etch rates in Å/cycle are also given in Table I. These etch rates were calculated using the MCPCs and an XRR density of 9.6 g/cm^3 for the HfO_2 ALD film. The ratio of ΔM_{TiCl_4}/MCPC is also listed in

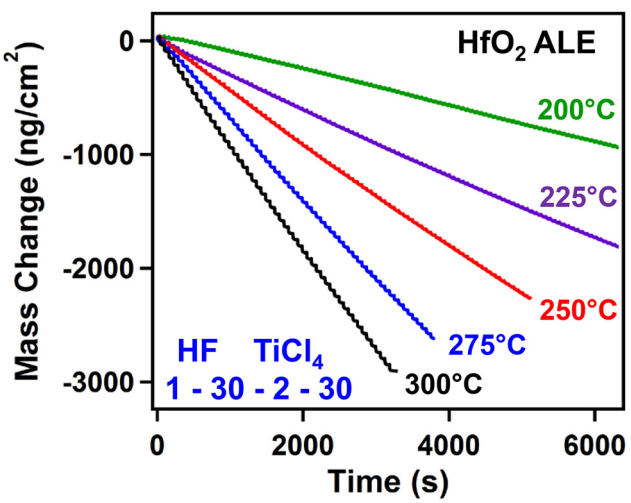

FIG. 5. Mass change vs time for Al_2O_3 ALE using sequential HF and $TiCl_4$ exposures at 200, 225, 250, 275, and 300 °C.

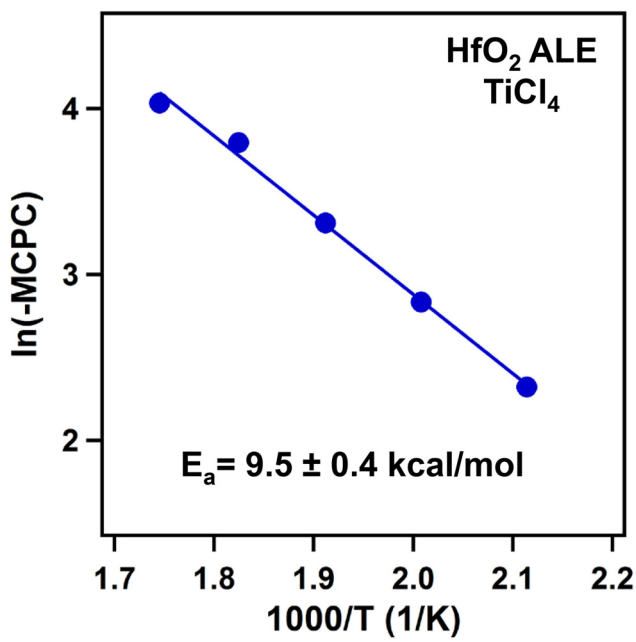

FIG. 7. Arrhenius plot of the MCPC. The slope yields an activation barrier of $E_a = 9.5$ kcal/mol.

TABLE I. MCPC, etch rate, ΔM_{HF}, ΔM_{TiCl_4}, ratio, x, and xMCPC for HfO_2 ALE at different temperatures.

Temperature (°C)	MCPC [ng/(cm^2 cycle)]	Etch rate (Å/cycle)	ΔM_{HF} [ng/(cm^2 cycle)]	ΔM_{TiCl_4} [ng/(cm^2 cycle)]	Ratio	x	xMCPC
200	−10.2	0.11	−10.1	−0.1	0	3.9	−39
225	−17.0	0.18	−7.5	−9.5	0.56	2.1	−35
250	−27.4	0.29	−5.9	−21.5	0.78	1.4	−38
275	−44.5	0.46	−2.5	−42.0	0.94	0.86	−38
300	−56.4	0.59	−1.3	−55.1	0.98	0.73	−41

Table I. This ratio was obtained during steady state HfO_2 ALE at 200–300 °C. This ratio can be used to understand the mechanism of the HfO_2 ALE reactions during the HF and $TiCl_4$ exposures.

C. Surface chemistry for HfO_2 ALE

The surface chemistry for HfO_2 ALE during the sequential HF and $TiCl_4$ exposures can be modeled as the following two reactions:

$$\text{(A) } HfO_2|xHfCl_4^* + (4+4x)HF \rightarrow HF_4|xHfF_4^* + 2H_2O + 4xHCl, \quad (4)$$

$$\text{(B) } HfF_4|xHfF_4^* + (1+x)TiCl_4 \rightarrow xHfCl_4^* + HfCl_4 + (1+x)TiF_4. \quad (5)$$

The parameter x designates the number of $HfCl_4$* species on the HfO_2 surface relative to the number of HfO_2 units that are etched during one HfO_2 ALE cycle. The asterisks designate the surface species, and the vertical lines distinguish the surface species from the underlying surface layer.

Equation (4) assumes that HF converts the HfO_2 and $HfCl_4$* surface species to HfF_4. The HF exposure removes all the Cl species. As mentioned in Sec. III A, $HfCl_4$ may not be the thermochemically favorable reaction product. The actual reaction product may be a mixed fluorine/chlorine species such as $HfF_{4-y}Cl_y$. However, $HfCl_4$ is employed in this surface chemical analysis for simplicity. Equation (5) assumes that $TiCl_4$ transfers Cl to the surface and does not leave any Ti species.

The overall proposed reaction can be described by

$$HfO_2 + (4+4x)\,HF + (1+x)TiCl_4 \rightarrow HfCl_4 + (1+x)TiF_4 + 2H_2O + 4xHCl. \quad (6)$$

MCPC is the total mass change per cycle and $MCPC = \Delta M_{TiCl_4} + \Delta M_{HF}$. The ratio of $\Delta M_{TiCl_4}/MCPC$ can be expressed as

$$\Delta M_{TiCl_4}/MCPC = (x(M_{HfCl_4} - M_{HfF_4}) - M_{HfF_4})/(-M_{HfO_2}). \quad (7)$$

M designates the molar mass in Eq. (7). x can then be obtained from the rearrangement of Eq. (7)

$$x = (M_{HfF_4} - M_{HfO_2}(\Delta M_{TiCl_4}/MCPC))/(M_{HfCl_4} - M_{HfF_4}). \quad (8)$$

The ratios for $\Delta M_{TiCl_4}/MCPC$ and the molar masses determine the x values for HfO_2 ALE that are given in Table I.

As defined above, x represents the number of $HfCl_4$* species on the HfO_2 surface relative to the number of HfO_2 units that are etched during one HfO_2 ALE cycle. For example, $x = 0.73$ for HfO_2 ALE at 300 °C. This x value indicates that there are 0.73 $HfCl_4$* surface species per HfO_2 species etched per HfO_2 ALE cycle. Table I reveals that x decreases as the reaction temperature increases.

In contrast to x, the product xMCPC is fairly constant at different reaction temperatures. The product xMCPC is 35–41 ng/cm^2 at 200–300 °C. This nearly constant value occurs because the HfO_2 etch rate increases while x decreases at higher reaction temperatures. This xMCPC value is proportional to the absolute $HfCl_4$* coverage during HfO_2 ALE. The nearly constant xMCPC values in Table I indicate that the absolute $HfCl_4$* coverage does not change significantly versus the reaction temperature.

The HfO_2 mass density of 9.6 g/cm^3 is equivalent to a number density of $\rho = 2.7 \times 10^{22}$ "HfO_2 units"/cm^3. Assuming a square lattice, this number density yields an estimate for the number of "HfO_2 units" on the HfO_2 surface of $\rho^{2/3} = 9.10 \times 10^{14}$ "HfO_2 units"/cm^2. This coverage of "HfO_2 units" is equivalent to an HfO_2 mass of 320 ng/cm^2. Using this HfO_2 mass as a reference, the xMCPC value of 35–41 ng/cm^2 is consistent with an $HfCl_4$* coverage that is equivalent to 11–13% of the HfO_2 units on the HfO_2 surface. Likewise, the Cl coverage is equivalent to 44–52% of the HfO_2 units on the HfO_2 surface.

D. Selectivity in ALE using HF and $TiCl_4$

Figure 8(a) displays the SE measurements of the film thicknesses for various thin films after 25, 50, 100, and 200 ALE cycles using sequential HF and $TiCl_4$ exposures at 250 °C. The HfO_2 and ZrO_2 films were etched linearly versus the number of ALE cycles. In contrast, there was no measurable thickness change for the Al_2O_3, SiO_2, Si_3N_4, and TiN films. There is a slight delay in the etching for HfO_2

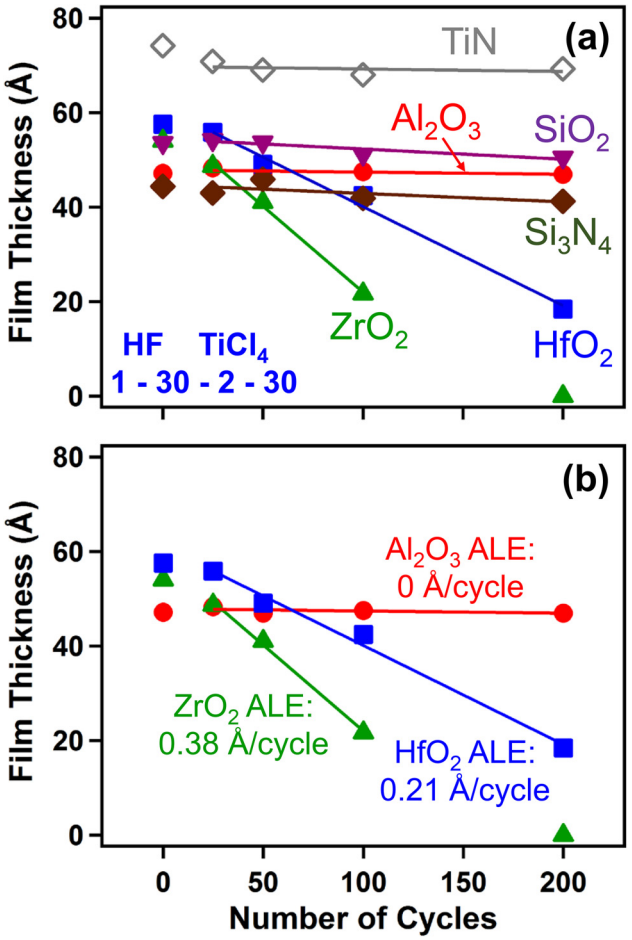

FIG. 8. (a) Film thickness vs the number of HF and $TiCl_4$ reaction cycles at 250 °C for a variety of materials. (b) Film thickness vs the number of HF and $TiCl_4$ reaction cycles at 250 °C for Al_2O_3, HfO_2, and ZrO_2 showing etch rates.

that may be related to surface cleanliness. All of the various films in Fig. 8(a) were in atmosphere prior to the etching experiments.

Figure 8(b) displays the film thickness versus the number of HF and $TiCl_4$ reaction cycles for the ZrO_2, HfO_2, and Al_2O_3 films. The linear least-squares fittings of the data in Fig. 8(b) yield etch rates of 0.38 and 0.21 Å/cycle for the ZrO_2 and HfO_2 films, respectively. In contrast, the Al_2O_3 film was not etched by the sequential HF and $TiCl_4$ exposures.

The observed selectivity in thermal ALE using HF and $TiCl_4$ as the reactants at 250 °C is very similar to the observed selectivity using HF and $SiCl_4$ as the reactants at 350 °C.[21] HfO_2 and ZrO_2 were both etched and Al_2O_3 was not etched using $SiCl_4$ and HF as the reactants.[21] Thermochemical calculations were employed to explain the lack of Al_2O_3 etching using HF and $SiCl_4$ as the reactants. Thermochemical calculations indicated that the ligand-exchange reaction of $SiCl_4$ with AlF_3 to yield SiF_4 and $AlCl_3$ was not favorable.[21] In contrast, the ligand-exchange reactions between $SiCl_4$ and ZrF_4 or HfF_4 to yield SiF_4 and $ZrCl_4$ or $HfCl_4$ were thermochemically favorable at >200 °C.[21]

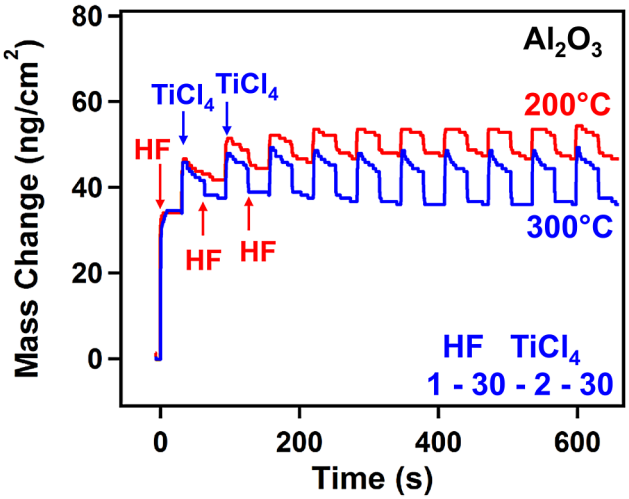

FIG. 9. Mass change vs time during ten sequential HF and $TiCl_4$ exposures on Al_2O_3 at 200 and 300 °C using the reaction sequence of (1−30−2−30).

Thermochemical calculations for the ligand-exchange reaction of $TiCl_4$ with AlF_3 assuming complete fluorine/chlorine exchange indicate that this reaction is not favorable. These thermochemical predictions are consistent with the experimental results that $TiCl_4$ with HF cannot etch Al_2O_3. However, the ligand-exchange reaction between $TiCl_4$ and ZrF_4 or HfF_4 is also not predicted to be thermochemically favorable. These thermochemical calculations assume that the ligand-exchange reactions produce complete fluorine/chlorine exchange. The disagreement between the thermochemical predictions and the experimental observations suggests that the ligand-exchange reaction may not produce complete fluorine/chlorine exchange. The $HfF_{4-y}Cl_y$ and $TiCl_{4-z}F_z$ etch products may have more favorable thermochemistry.

Additional experiments were performed to understand the lack of Al_2O_3 etching during sequential HF and $TiCl_4$ exposures. Figure 9 displays the mass change versus time during ten sequential HF and $TiCl_4$ exposures on Al_2O_3 at 200 and 300 °C using the reaction sequence of (1−30−2−30). The HF exposure on Al_2O_3 yielded a mass gain of $\Delta M_{HF} = 33–35$ ng/cm^2. This mass gain is consistent with the fluorination of the Al_2O_3 film: $Al_2O_3 + 6HF \rightarrow 2AlF_3 + 3H_2O$. There is an additional mass gain during the $TiCl_4$ exposure that could be attributed to the replacement of AlF* surface species with AlCl* surface species. In addition, the mass gain may result from the adsorption of $TiCl_4$ on the AlF_3 surface possibly as $TiCl_3$* or Cl* surface species. The next HF exposure then could exchange chlorine for fluorine by $AlCl^* + HF \rightarrow AlF^* + HCl$ or possibly remove the $TiCl_3$* and Cl* surface species by $TiCl_3^* + Cl^* + 4HF \rightarrow TiF_4 + 4HCl$. The results in Fig. 9 confirm that HF and $TiCl_4$ exposures have no ability to etch Al_2O_3 at 250 °C.

E. Al_2O_3 as an etch stop for HfO_2 ALE

Figure 10 shows the mass change during the growth of an Al_2O_3/HfO_2 ALD bilayer followed by HfO_2 ALE using HF

and $TiCl_4$ at 250 °C. The bilayer composed of 10 Å Al_2O_3 and 16 Å HfO_2 was grown using 10 Al_2O_3 ALD cycles and 20 HfO_2 ALD cycles. This bilayer was used to study the HfO_2 ALE at the interface with the Al_2O_3 film. TMA and TDMAH were utilized with H_2O for Al_2O_3 ALD and HfO_2 ALD using the reaction sequence of 1−30−1−30. HfO_2 ALE was then performed using HF and $TiCl_4$ as the reactants. The HfO_2 ALE cycles were performed using 80 sequential HF and $TiCl_4$ exposures with a reaction sequence of 1−30−2−30.

Approximately one-half of the HfO_2 film was etched in ~20 HfO_2 ALE cycles. Figure 10 shows that the etch rate slowed down as the surface of the HfO_2 film reaches the interface with the Al_2O_3 film. Relative to the mass change of ~300 ng/cm^2 at the initiation of HfO_2 ALD, the etch rate during HfO_2 ALE begins to be reduced at a mass change of ~700 ng/cm^2 or a HfO_2 mass per area of ~400 ng/cm^2. This HfO_2 mass per area is consistent with ~4 Å of HfO_2 or approximately one monolayer of HfO_2 thickness. The etch is then stopped at a HfO_2 mass per area of ~150 ng/cm^2. This HfO_2 mass per area is close to the interface between HfF_4 and Al_2O_3. The fluorination of Al_2O_3 could be responsible for a mass gain of 35 ng/cm^2. Therefore, the remaining mass per area of 115 ng/cm^2 corresponds to ~1.7 Å of HfF_4 using the mass density of 6.8 g/cm^3 for HfF_4.[45] The likely HfF_4/AlF_3 interfacial alloy may be difficult to remove using HF and $TiCl_4$ because $TiCl_4$ cannot remove the AlF_3 layer. The Al_2O_3 underlayer acts as an effective etch stop for HfO_2 ALE.

F. $TiCl_4$ as a metal reactant for thermal ALE

$TiCl_4$ is a useful metal reactant for thermal ALE. Together with HF as the fluorination reactant, TiC_4 can etch HfO_2 over a wide range of temperatures from 200 to 300 °C. In contrast, $Al(CH_3)_3$ and $SiCl_4$ as metal reactants together with HF require higher temperatures to obtain similar etch rates for HfO_2.[21] HF and $TiCl_4$ also have a comparable etch rate to the etch rate from HF and $Sn(acac)_2$ at 200 °C.[21] In addition, $Sn(acac)_2$ suffers from thermal decomposition and inconsistent pressure transients over time when held at a source temperature of 100 °C.

HF and $TiCl_4$ can selectively etch HfO_2 and ZrO_2 in the presence of Al_2O_3, SiO_2, Si_3N_4, and TiN. The ability of HF and $TiCl_4$ to etch only HfO_2 and ZrO_2 and not Al_2O_3 is similar to the selectivity observed for HF and $SiCl_4$.[21] In comparison, $Sn(acac)_2$ and $AlCl(CH_3)_2$ with HF can selectively etch HfO_2, ZrO_2, and Al_2O_3 in the presence of SiO_2, Si_3N_4, and TiN.[21] HF and $Al(CH_3)_3$ can selectively etch Al_2O_3 and HfO_2 in the presence of ZrO_2, SiO_2, Si_3N_4, and TiN.[21]

Different metal reactants and fluorination reactants will be required to etch selectively one material or several materials in the presence of various different materials. This etch selectivity will be required for area selective deposition and area selective etch.[5] Additional studies of other metal reactants and fluorination reactants are needed to obtain this desired selectivity. This selectivity will require a detailed understanding of the underlying surface chemistry during thermal ALE. In addition, higher levels of selectivity may also need new etching mechanisms or procedures to block etching that are material specific.

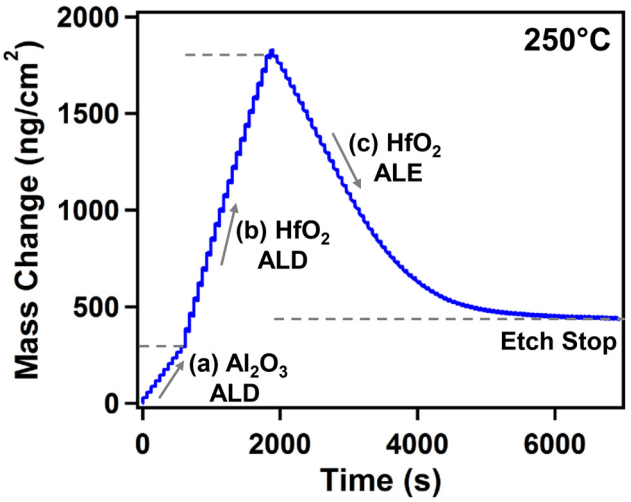

FIG. 10. Mass change vs time during (a) 10 Al_2O_3 ALD cycles using sequential TMA and H_2O exposures (1−30−1−30) and (b) 20 HfO_2 ALD cycles using sequential TDMAH and H_2O exposures (1−30−1−30) and 80 HfO_2 ALE cycles using sequential HF and $TiCl_4$ exposures (1−30−2−30) at 250 °C.

IV. CONCLUSIONS

$TiCl_4$ was used as a new metal chloride reactant for thermal HfO_2 ALE. *In situ* QCM measurements were used to study thermal HfO_2 ALE using HF and $TiCl_4$ as the reactants from 200 to 300 °C. The QCM measurements revealed that the HfO_2 film thicknesses were etched linearly versus the number of HF and $TiCl_4$ reaction cycles. The individual HF and $TiCl_4$ reactions were also self-limiting versus HF and $TiCl_4$ exposures. MCPCs of −10.2 ng/(cm^2 cycle) at 200 °C and −56.4 ng/(cm^2 cycle) at 300 °C were obtained from the QCM measurements. Based on the HfO_2 film density of 9.6 g/cm^3, these MCPCs are equivalent to HfO_2 etch rates of 0.11 Å/cycle at 200 °C and 0.59 Å/cycle at 300 °C.

SE measurements were also employed to survey the etching of various materials and to determine the selectivity of thermal ALE using HF and $TiCl_4$ as the reactants. The SE results revealed selective etching. HfO_2 and ZrO_2 were etched by HF and $TiCl_4$. In contrast, Al_2O_3, SiO_2, Si_3N_4, and TiN were not etched by HF and $TiCl_4$. The reaction thermochemistry and the stability and volatility of the possible etch products can explain the observed selectivity. Based on the selectivity between HfO_2 and Al_2O_3, Al_2O_3 can serve as an etch stop for HfO_2 ALE.

ACKNOWLEDGMENTS

This work was funded by the Intel Corporation through the Semiconductor Research Corporation (SRC). Additional support was provided by the National Science Foundation through Grant No. CHE-1609554. The authors thank Scott Clendenning and Cen Tan from Intel Corporation for useful discussions.

[1]K. J. Kanarik, T. Lill, E. A. Hudson, S. Sriraman, S. Tan, J. Marks, V. Vahedi, and R. A. Gottscho, J. Vac. Sci. Technol. A **33**, 020802 (2015).
[2]G. S. Oehrlein, D. Metzler, and C. Li, ECS J. Solid State Sci. Technol. **4**, N5041 (2015).
[3]T. Faraz, F. Roozeboom, H. C. M. Knoops, and W. M. M. Kessels, ECS J. Solid State Sci. Technol. **4**, N5023 (2015).
[4]S. M. George and Y. Lee, ACS Nano **10**, 4889 (2016).
[5]C. T. Carver, J. J. Plombon, P. E. Romero, S. Suri, T. A. Tronic, and R. B. Turkot, ECS J. Solid State Sci. Technol. **4**, N5005 (2015).
[6]S. D. Athavale and D. J. Economou, J. Vac. Sci. Technol. B **14**, 3702 (1996).
[7]S. D. Park, D. H. Lee, and G. Y. Yeom, Electrochem. Solid State Lett. **8**, C106 (2005).
[8]H. Sakaue, S. Iseda, K. Asami, J. Yamamoto, M. Hirose, and Y. Horiike, Jpn. J. Appl. Phys. **29**, 2648 (1990).
[9]T. Sugiyama, T. Matsuura, and J. Murota, Appl. Surf. Sci. **112**, 187 (1997).
[10]W. S. Lim, S. D. Park, B. J. Park, and G. Y. Yeom, Surf. Coat. Technol. **202**, 5701 (2008).
[11]S. D. Park, C. K. Oh, J. W. Bae, G. Y. Yeom, T. W. Kim, J. I. Song, and J. H. Jang, Appl. Phys. Lett. **89**, 043109 (2006).
[12]D. Metzler, R. L. Bruce, S. Engelmann, E. A. Joseph, and G. S. Oehrlein, J. Vac. Sci. Technol. A **32**, 020603 (2014).
[13]D. Metzler, C. Li, S. Engelmann, R. L. Bruce, E. A. Joseph, and G. S. Oehrlein, J. Vac. Sci. Technol. A **34**, 01b101 (2016).
[14]W. H. Kim, D. Sung, S. Oh, J. Woo, S. Lim, H. Lee, and S. F. Bent, J. Vac. Sci. Technol. A **36**, 01b104 (2018).
[15]C. Li, D. Metzler, C. S. Lai, E. A. Hudson, and G. S. Oehrlein, J. Vac. Sci. Technol. A **34**, 041307 (2016).
[16]J. B. Park, W. S. Lim, B. J. Park, I. H. Park, Y. W. Kim, and G. Y. Yeom, J. Phys. D: Appl. Phys. **42**, 055202 (2009).
[17]S. D. Park, W. S. Lim, B. J. Park, H. C. Lee, J. W. Bae, and G. Y. Yeom, Electrochem. Solid State Lett. **11**, H71 (2008).
[18]Y. Y. Kim, W. S. Lim, J. B. Park, and G. Y. Yeom, J. Electrochem. Soc. **158**, D710 (2011).
[19]E. Vogli, D. Metzler, and G. S. Oehrlein, Appl. Phys. Lett. **102**, 253105 (2013).
[20]Y. Lee and S. M. George, ACS Nano **9**, 2061 (2015).
[21]Y. Lee, C. Huffman, and S. M. George, Chem. Mater. **28**, 7657 (2016).
[22]J. W. DuMont, A. E. Marquardt, A. M. Cano, and S. M. George, ACS Appl. Mater. Interfaces **9**, 10296 (2017).
[23]Y. Lee, J. W. DuMont, and S. M. George, Chem. Mater. **27**, 3648 (2015).
[24]Y. Lee, J. W. DuMont, and S. M. George, Chem. Mater. **28**, 2994 (2016).
[25]Y. Lee, J. W. DuMont, and S. M. George, ESC J. Solid State Sci. Technol. **4**, N5013 (2015).
[26]Y. Lee, J. W. DuMont, and S. M. George, J. Phys. Chem. C **119**, 25385 (2015).
[27]N. R. Johnson, H. Sun, K. Sharma, and S. M. George, J. Vac. Sci. Technol. A **34**, 050603 (2016).
[28]D. R. Zywotko and S. M. George, Chem. Mater. **29**, 1183 (2017).
[29]N. R. Johnson and S. M. George, ACS Appl. Mater. Interfaces **9**, 34435 (2017).
[30]Y. Lee and S. M. George, Chem. Mater. **29**, 8202 (2017).
[31]W. Xie, P. C. Lemaire, and G. N. Parsons, ACS Appl. Mater. Interfaces **10**, 9147 (2018).
[32]J. K. C. Chen, N. D. Altieri, T. Kim, E. Chen, T. Lill, M. H. Shen, and J. P. Chang, J. Vac. Sci. Technol. A **35**, 05c305 (2017).
[33]P. C. Lemaire and G. N. Parsons, Chem. Mater. **29**, 6653 (2017).
[34]J. H. Choi, Y. Mao, and J. P. Chang, Mater. Sci. Eng. R **72**, 97 (2011).
[35]K. Mistry *et al.*, *2007 IEEE International Electron Devices Meeting*, Washington, DC, 10–12 December 2007 (IEEE, 2007), Vols. 1 and 2, p. 247.
[36]A. Tsormpatzoglou, D. H. Tassis, C. A. Dimitriadis, M. Mouis, G. Ghibaudo, and N. Collaert, Semicond. Sci. Technol. **24**, 125001 (2009).
[37]D. W. Wang, Q. Wang, A. Javey, R. Tu, H. J. Dai, H. Kim, P. C. McIntyre, T. Krishnamohan, and K. C. Saraswat, Appl. Phys. Lett. **83**, 2432 (2003).
[38]G. A. Olah, M. Nojima, and I. Kerekes, Synthesis-Stuttgart **12**, 779 (1973).
[39]Y. Lee, J. W. DuMont, A. S. Cavanagh, and S. M. George, J. Phys. Chem. C **119**, 14185 (2015).
[40]J. W. Elam, M. D. Groner, and S. M. George, Rev. Sci. Instrum. **73**, 2981 (2002).
[41]R. D. Shannon, R. C. Shannon, O. Medenbach, and R. X. Fischer, J. Phys. Chem. Ref. Data **31**, 931 (2002).
[42]*HSC Chemistry*, HSC Chemistry 5.1, Outokumpu Research Oy, Pori, Finland.
[43]B. E. Deal and A. S. Grove, J. Appl. Phys. **36**, 3770 (1965).
[44]E. H. Hall, J. M. Blocher, and I. E. Campbell, J. Electrochem. Soc. **105**, 275 (1958).
[45]Y. Lee, H. X. Sun, M. J. Young, and S. M. George, Chem. Mater. **28**, 2022 (2016).